Pergamon

Int. J. Solids Structures Vol. 34, No. 29, pp. 3885–3901, 1997

0020-7683/97 $17.00 + .00

PII: S0020-7683(96)00197-7

MATERIAL INTERFACE INSPECTION BY LAMB WAVES

T. KUNDU
Department of Civil Engineering and Engineering Mechanics, University of Arizona, Tucson, AZ 85721, U.S.A.

and

K. MASLOV
Semienov Institute of Chemical Physics, Russian Academy of Science, Moscow 117334, Russia

(*Received* 25 *January* 1996; *in revised form* 6 *August* 1996)

Abstract—In this paper an investigation on the Lamb wave propagation through a two-layered glass plate with different interface conditions between the layers is carried out to study the effectiveness of Lamb waves in detecting defects at the interface as well as estimating the interface strength. To this end the stress field inside the two layered plate is theoretically calculated for different interface conditions and for a number of propagating Lamb modes. It is observed that, for every Lamb mode, the stress field inside the plate varies significantly with depth. Symmetric modes generate maximum normal stress and zero shear stress at the central plane; the situation is reversed for the antisymmetric modes. it is found that the Lamb modes which produce large shear stress at the interface position are most sensitive to the shear stiffness of the interface. Void and delamination type defects that release the interface stress affect those Lamb modes most significantly which produce high stress at the interface position. Theoretical predictions have been experimentally verified. © 1997 Elsevier Science Ltd.

INTRODUCTION

It is well known that the longitudinal wave reflection coefficient is not very effective in characterizing an interface or determining its shear stiffness and strength. Shear wave reflection coefficient is much more sensitive to the interface condition [Jiao and Rose (1991), Matikas and Karpur (1993)]. Since different Lamb wave modes generate high normal and shear stresses at various depths of the plate it is expected that some Lamb modes will be very sensitive to the interface defects as well as its stiffness and strength. In this paper it is studied how sensitive the Lamb modes are to the interface conditions.

Many investigators studied the Lamb wave propagation characteristics for material characterization and related the dispersion curves and attenuation coefficient to the material properties, as noted by Kundu *et al.* (1996). In recent years a few have also attempted to scan a specimen using Lamb waves to generate the image of internal defects [Chimenti and Martin (1991), Karpur *et al.* (1995), Kundu *et al.* (1996), Maslov and Kundu (1997)]. Kundu *et al.* (1996) have experimentally demonstrated how Lamb wave generated images have several advantages over the longitudinal wave generated images as conventionally done in C-scan ultrasonic imaging.

In the present paper an attempt is made to use the Lamb waves for characterizing interfaces. This is done by theoretically computing the internal stress field inside a two layered glass plate with an interface and studying the variation of the stress field for different Lamb modes. Three types of interfaces are studied, slip, rigid (no-slip) and glued (elastic). A slip interface has no shear stiffness and strength but normal stiffness is the same as the adjacent layers, in this case glass, a rigid interface has normal and shear stiffnesses the same

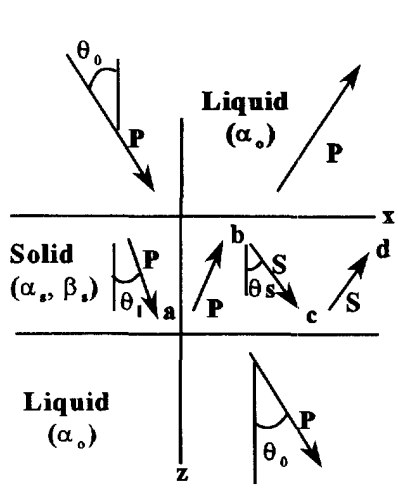

Fig.1a

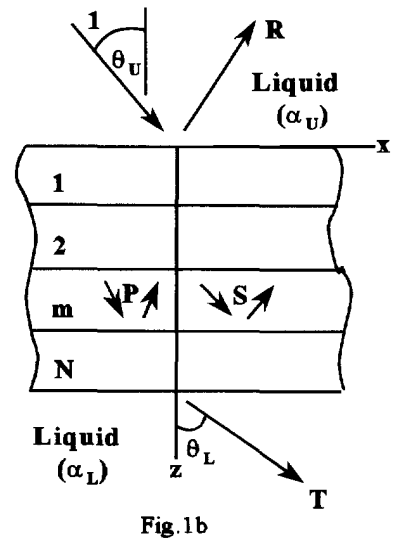

Fig.1b

Fig. 1. (a) Different waves in a homogeneous plate and in the surrounding liquid. (b) Waves in the liquid and in different layers of a multilayered plate.

as the adjacent layers, and a glued interface has shear and normal stiffnesses the same as the glue, typically less than the glass.

THEORY

For computing internal stresses in the plate, one needs to study the mechanics of elastic wave propagation in a multilayered solid. A number of investigators over the last few decades have studied this problem. Thomson (1950), Haskell (1953), Dunkin (1965), Schwab and Knopoff (1970), Kundu and Mal (1985), Mal (1988), Mal *et al.* (1991), Lévesque and Piché (1992), Taylor and Nayfeh (1992), Yang and Kundu (1997), among others, studied various aspects of this problem. A good review of some of these investigations can be found in Brekhovskikh and Godin (1990). Since the fundamental theory of elastic wave propagation in single and multilayered plates is well developed, only a brief description of that theory which is relevant to our problem is given here, following Brekhovskikh and Godin (1990).

Let us consider the two dimensional elastic wave propagation problem in the xz plane as shown in Fig. 1a. the P and SV wave potentials, denoted by ϕ and ψ, respectively, can be expressed in the forms shown below,

$$\phi = [ae^{i\nu z} + be^{-i\nu z}]e^{ikx - i\omega t}$$
$$\psi = [ce^{i\eta z} + de^{-i\eta z}]e^{ikx - i\omega t} \tag{1}$$

where the wave number $k = (\omega/\alpha_0)\sin(\theta_0) = (\omega/\alpha_s)\sin(\theta_1) = (\omega/\beta_s)\sin(\theta_s)$, $\nu = (\omega/\alpha_s)\cos(\theta_1)$, $\eta = (\omega/\beta_s)\cos(\theta_s)$, ω is the signal frequency in rad/sec, α_0, α_s and β_s are longitudinal wave speed in water, longitudinal wave speed in solid and shear wave speed in solid, respectively. For brevity, in the subsequent expressions the common factor $e^{ikx - i\omega t}$ is omitted.

The particle displacement can be obtained from the wave potentials,

$$u_x = ik\phi - \frac{\partial \psi}{\partial z}$$
$$u_z = \frac{\partial \phi}{\partial z} + ik\psi \tag{2}$$

and the stress components are given by

$$\sigma_{xz} = -2\rho k\beta_s^2\left(\gamma\psi - i\frac{\partial\phi}{\partial z}\right)$$

$$\sigma_{zz} = 2\rho k\beta_s^2\left(\gamma\phi + i\frac{\partial\psi}{\partial z}\right)$$

$$\sigma_{xx} = 2(\sigma_{zz} + 2ik\rho\beta_s^2 u_x)\left(1 - \frac{\beta_s^2}{\alpha_s^2}\right) - \sigma_{zz} \tag{3}$$

where $\gamma = k - \omega^2/(2k\beta_s^2)$.

For a multilayered plate immersed in water, as shown in Fig. 1b, we can assign a superscript 'm' to displacement and stress components to indicate that they correspond to the m-th layer. From the continuity of normal and shear stresses and displacements across the interface between two adjacent elastic layers one can relate the displacement-stress vectors of any two layers in the following form

$$\begin{bmatrix} u_x^m \\ u_z^m \\ \sigma_{zz}^m \\ \sigma_{xz}^m \end{bmatrix} = A_m \cdot A_{m+1} \cdot A_{m+2} \cdots A_{n-1} \begin{bmatrix} u_x^n \\ u_z^n \\ \sigma_{zz}^n \\ \sigma_{xz}^n \end{bmatrix} \tag{4}$$

where A_m is a 4×4 layer matrix or propagator matrix of the m-th layer. The superscripts 'm' and 'n' of the elements of the displacement-stress vectors of eqn (4) correspond to the m-th and n-th layers, respectively. Expressions for the individual elements of the layer matrix can be found in Thomson (1950), Haskell (1953), or Brekhovskikh and Gobin (1990) and are omitted.

If fluid half-spaces are present above and below the multilayered plate, as shown in Fig. 1b, then wave potentials for the upper and lower half-spaces can be written as

$$\phi_U = e^{-i\nu_U z} + Re^{i\nu_U z}$$

$$\phi_L = Te^{-i\nu_L z} \tag{5}$$

where 'R' and 'T' are plane wave reflection and transmission coefficients of the multilayered plate, immersed in the fluid; subscripts U and L of ν indicate upper and lower fluid half-spaces, respectively.

To compute the stress and displacement components inside the plate, their values at the top and bottom liquid-solid interfaces are to be obtained first. It should be noted here that $\sigma_{xz} = 0$ at both top and bottom liquid-solid interfaces, and u_z, σ_{zz} are continuous across both these interfaces, so that their values can be computed in terms of R and T from the fluid potentials given in eqn (5) and displacement/stress-potential relations given in eqns (2) and (3). Since horizontal displacements on the fluid and solid sides of the interface are not necessarily the same, because of possible slippage at the interface, two horizontal components of displacement at the top and bottom surfaces of the plate are unknown, along with R and T. These four unknowns are solved from the four scalar equations given in (4). Thus, we get

$$R = \frac{M_{32} - i\omega Z_L M_{33} + i\omega Z_U(M_{22} - i\omega Z_L M_{23})}{M_{32} - i\omega Z_L M_{33} - i\omega Z_U(M_{22} - i\omega Z_L M_{23})}$$

$$T = \frac{-2i\omega Z_L \rho_U/\rho_L}{M_{32} - i\omega Z_L M_{33} - i\omega Z_U(M_{22} - i\omega Z_L M_{23})} \tag{6}$$

where $M_{ij} = J_{ij} - J_{i1}J_{4j}/J_{41}$, J is a 4×4 matrix obtained by multiplying layer matrices of all layers. $Z_L = \rho_L \alpha_L / \cos\theta_L$ and $Z_U = \rho_U \alpha_U / \cos\theta_U$ are the acoustic impedances of the lower and upper fluid half spaces, respectively. After computing the stress and displacement components at the top and bottom surfaces of the plate, their values at any other interface inside the plate can be obtained from eqn (4). To get these values at a point within a layer, an artificial boundary can be introduced that goes through that point, and then eqn (4) can be used.

The above derivation can be followed for a multilayered solid plate. However, if there is a liquid layer in between two solid layers then the details of the formulation vary since the continuity conditions across a liquid-solid interface are different from those across a solid-solid interface. Readers interested in this formulation are referred to Kundu (1992) for a detailed derivation.

It is well-known that the above formulation (with or without a liquid layer) works well for low frequencies or thin plates, however, they suffer from a severe numerical loss-of-precision problem as the frequency or the plate thickness increases. To avoid the precision problem at high frequencies the delta matrix modification (Dunkin, 1965; Kundu and Mal, 1985; Lévesque and Piché, 1992) must be adopted.

NUMERICAL AND EXPERIMENTAL RESULTS

First we compute the Lamb wave dispersion curves and stress fields for different Lamb modes inside a two-layered glass plate for three different interface conditions—slip (wet contact), rigid (no-slip or perfect contact), and glued (elastic contact), as shown in Figs 2a, b and c, respectively. These three specimens which were fabricated for this investigation will be identified as specimens 2a, 2b and 2c, respectively. For the glued interface (specimen 2c) a scratch (approximately 0.1 mm deep) was created on one glass surface adjacent to the interface as shown in Fig. 2c. For carrying out the theoretical analysis, the elastic wave speeds, densities and dimensions of glass, water and glue layers are required. These are given in Table 1.

A special brass chamber was fabricated in which the glass slides can be placed and a hydraulic pressure can be applied to control the interface thickness between the glass slides. A cross section of the chamber is shown in Fig. 3. The upper brass block has a square hole through which transducer generated ultrasonic signal can travel to the plate and the reflected signal can travel back to the receiver. The bottom block has a square chamber with a rubber O-ring seal. It is possible to apply controlled pressure in this chamber to monitor the distance between the two slides.

Figure 4 shows the Lamb wave dispersion curves for the two layered plate with a slip interface (Fig. 2a) between the two plates. The solid and dashed lines correspond to the symmetric and antisymmetric modes, respectively. To compute the theoretical Lamb wave dispersion curves, first the reflection coefficient (eqn 5) for different frequencies are computed for a number of angles of incidence. The angle of incidence and the Lamb wave phase velocity are related by Snell's law,

$$C_L = \frac{\alpha_U}{\sin\theta} \tag{7}$$

where C_L is the Lamb wave phase velocity, θ is the angle of incidence and α_U is the longitudinal wave speed in water. For a fixed angle of incidence, if Lamb waves are generated at some frequencies then dips in the reflection spectra are observed at those frequencies. Dispersion curves in Fig. 4 are obtained by plotting those dips for different phase velocities. Circles (○) in Fig. 4 are experimental data points. Excellent matching between theoretical and experimental results should be noted here.

Lamb waves are generated and detected experimentally by placing two transducers in the pitch-catch arrangement and then exciting the transmitter in the tone-burst mode by continuously varying the signal frequency. If the specimen is located at the focus position

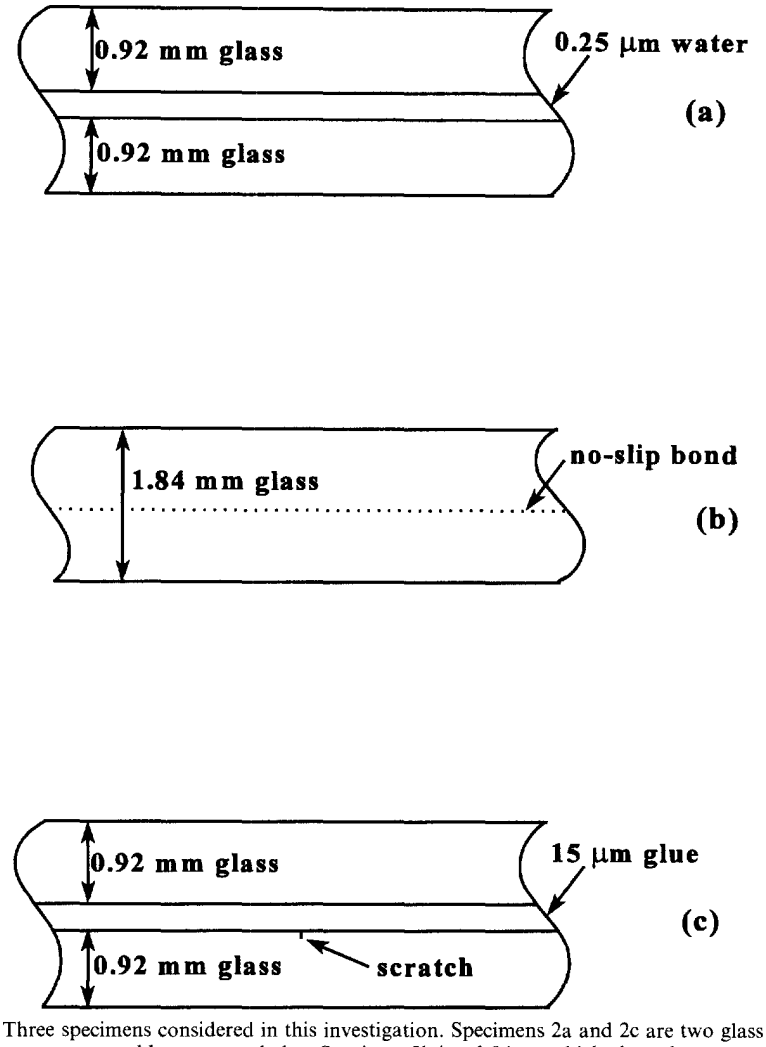

Fig. 2. Three specimens considered in this investigation. Specimens 2a and 2c are two glass plates connected by water and glue. Specimen 2b is a 1.84 mm thick glass plate.

then dips in the reflection spectra correspond to the Lamb modes, on the other hand if the reflecting surface is located between the focal point and the transducers then peaks in the reflection spectra correspond to the Lamb modes. For a detailed discussion of the experimental technique for generating and detecting Lamb waves one is referred to Kundu *et al.* (1996) or Maslov and Kundu (1997).

To investigate if Lamb wave dispersion curves can distinguish slip bonds from rigid bonds the dispersion curves are theoretically computed for a 1.84 mm thick glass plate (specimen 2b) and plotted in Fig. 5. Solid and dashed lines correspond to symmetric and antisymmetric modes respectively. Symmetric modes of Fig. 4 match very well with the symmetric modes of Fig. 5, however antisymmetric modes show some difference. These modes for specimen 2a are again plotted in Fig. 5 by stars (★). Clearly, symmetric modes

Table 1. List of material properties and dimensions of different layers

Layer material	Thickness (mm)	ρ (gm/cc)	α (km/sec)	β (km/sec)
Glass	0.92	2.25	5.66	3.4
Glue (Epoxy)	0.015	1.25	2.8	1.2
Water	<0.00025	1.0	1.49	0.0

where ρ, α, and β are density, P-wave speed and S-wave speed, respectively. Properties for glass and water are measured in the laboratory and those for the glue are taken from Briggs (1992). The water layer thickness was less than 0.25 micron at the interface and was controlled optically by interference rings.

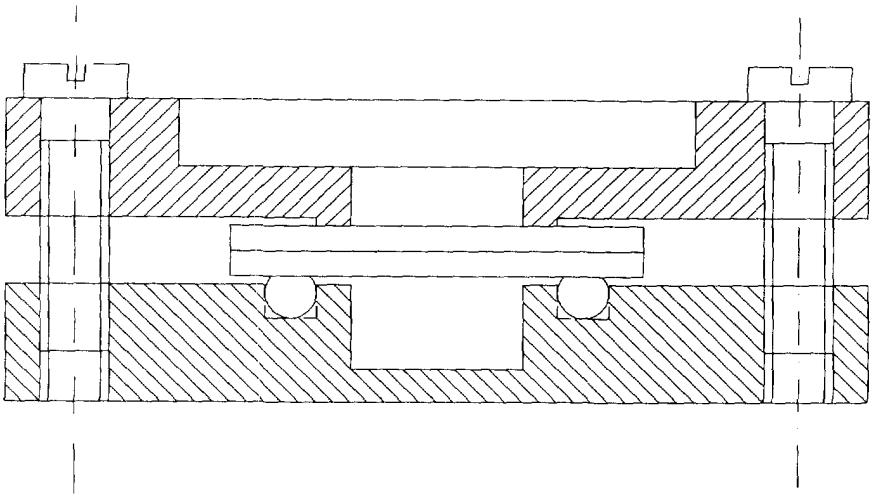

Fig. 3. Brass chamber, in which the specimens were placed during the ultrasonic scanning.

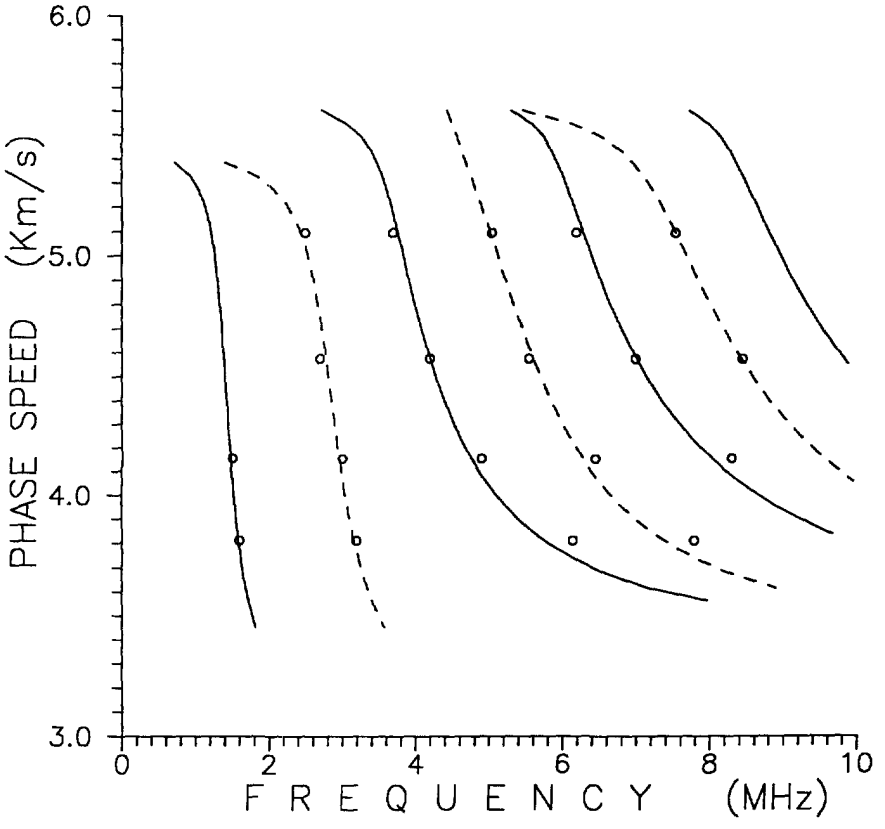

Fig. 4. Theoretical Lamb wave dispersion curves for specimen 2a. Solid and dashed lines show the symmetric and antisymmetric modes respectively. Circles (○) are experimental data points.

are not very sensitive to the interface stiffness/strength but antisymmetric modes are. That is why symmetric modes show no change when the slip interface is replaced by the rigid interface but antisymmetric modes show some variation.

If one wants to provide theoretical justification of these results one needs to compute the internal stress fields of the plates with rigid and slip bonds for symmetric and antisymmetric Lamb modes. Figures 6a and 6b show the shear stress σ_{xz} inside the plate for slip and rigid bonds, respectively. Both plots are for the first antisymmetric (A_1) mode. In these plots the plate thickness has been normalized. Hence, 0 to 1 along the depth axis

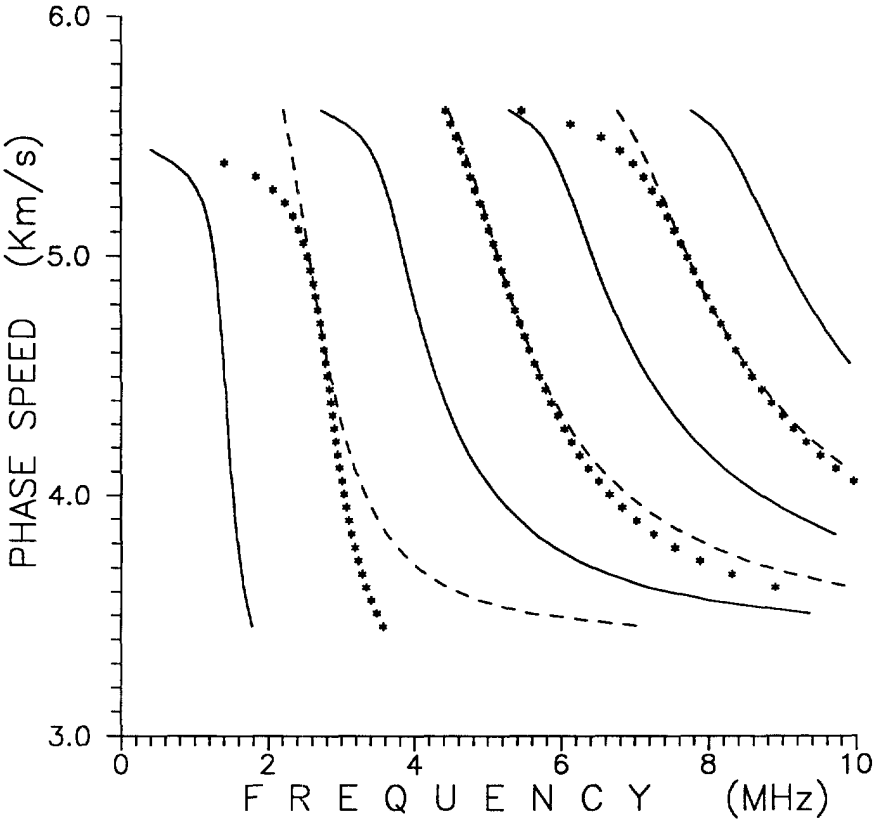

Fig. 5. Theoretical Lamb wave dispersion curves for specimen 2b. Solid and dashed lines show the symmetric and antisymmetric modes respectively. Stars (★) correspond to the antisymmetric modes of specimen 2a. Symmetric modes of specimens 2a and 2b coincide.

corresponds to 0 to 1.84 mm for the rigid bond (specimen 2b) and 0 to 1.84025 mm for the slip bond (specimen 2a). It should be noted here that the shear stress is large (Fig. 6b) at the rigid interface position for the A_1 mode, and it goes down to zero for the slip bond (Fig. 6a). Naturally, this mode is sensitive to the shear stiffness of the interface. It should also be noted here that for the phase velocity, 4.5–5 km/sec shear stress at the interface position is small for both rigid and slip bonds and hence, no significant difference in this mode for rigid and slip bonds is observed in the dispersion curve of Fig. 5 for the phase velocity between 4.5 and 5 km/sec.

Shear stress distribution for the second antisymmetric (A_2) mode also shows large stress at the central plane of specimen 2b (Fig. 6d) and small stress at the same location for specimen 2a (Fig. 6c) for the phase velocity less than 4.5 km/sec. In this region, the A_2 mode dispersion curve of Fig. 5 also shows differences for slip and rigid bonds.

The stress distribution for symmetric modes, on the other hand, does not show significant differences between slip bonded and rigid bonded plates. Figures 7a and 7b show the shear stress patterns for the first symmetric (S_1) mode, for slip and rigid bonded plates, respectively. Normal stress distributions for these two interface conditions for the same (S_1) mode are shown in Figs 7c and 7d. Clearly for both interface conditions the shear stress is zero at the interface and the normal stress is maximum there. Hence this mode cannot distinguish slip bonds from rigid bonds. This is because slip bonds cannot transmit the shear stress but can easily transmit the normal stress. For the same reason longitudinal waves often propagates through the fluid filled slip bonds completely missing them during the conventional C-scan ultrasonic inspection.

Dispersion curves for the glued plate (specimen 2c) are shown in Fig. 8. Solid and dashed lines correspond to the theoretically computed symmetric and antisymmetric modes, respectively. Circles are experimental data points. Again, matching between theoretical and experimental results is excellent.

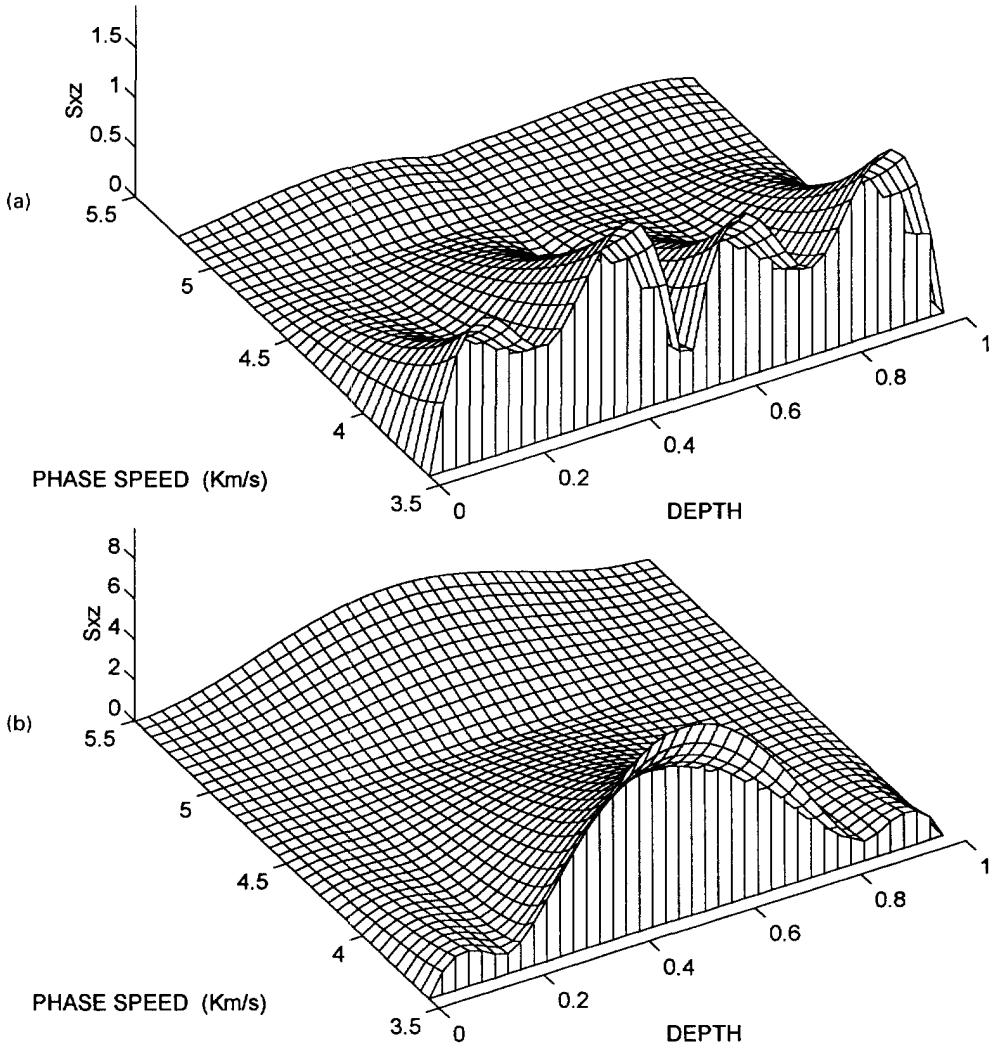

Fig. 6. Variations of σ_{xz} for A_1 (Figs 6a and 6b) and A_2 (Figs 6c and 6d) modes in specimens 2a (Figs 6a and 6c) and 2b (Figs. 6b and 6d).

Shear and normal stress distributions in this plate for the first antisymmetric mode (A_1) are shown in Figs 9a and 9b, respectively. Those for the A_2 mode are shown in Figs 9c and 9d respectively. Note that, for the A_1 mode, the shear stress at the central plane (glued interface) is high, neither zero as in the slip bonded interface nor a maximum as in the rigid interface. For the A_2 mode, the shear stress is also nonzero at the central plane, however, it is not as large as that for the A_1 mode. Shear and normal stress distributions in the same plate for the first symmetric (S_1) mode are shown in Figs 10a and 10b. As expected, the normal stress is zero at the central plane (glued interface) for antisymmetric modes and shear stress is zero at the same location for the symmetric mode.

Figure 11a shows a number of images of the glued plate, generated by different Lamb modes—A_1 (top row), S_1 (middle row) and A_2 (bottom row). Three columns correspond to three different incident angles—17° (corresponding phase velocity is 5.1 km/sec, left column), 19° (phase velocity is 4.58 km/sec, middle column), and 21° (phase velocity is 4.16 km/sec, right column). Note that the interface defect generated by the scratch can be clearly seen in the S_1 mode images and can be faintly seen in A_1 and A_2 images only for the 21° incident angle. This observation can be explained from the computed stress field in the following manner. S_1 mode produces high normal stress at the interface. The scratch

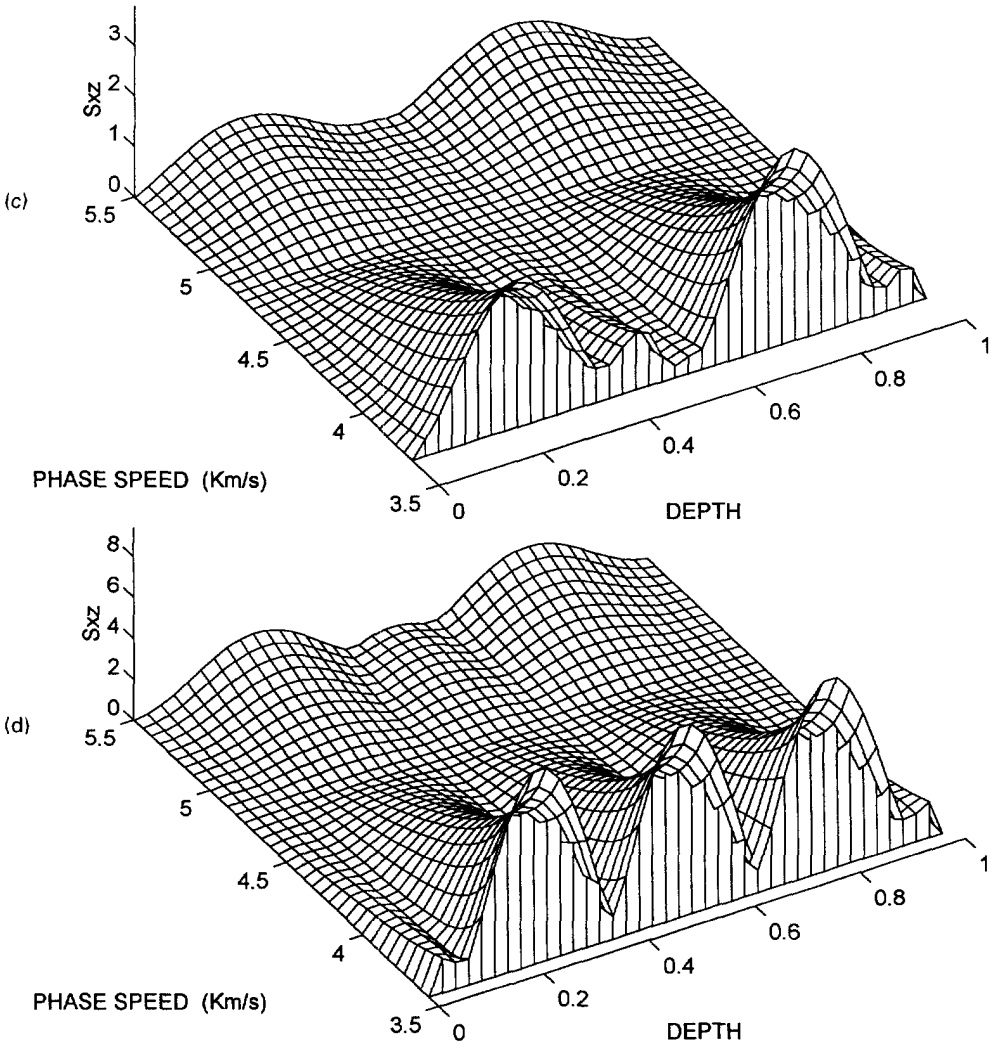

Fig. 6.—*Continued.*

releases the normal stress and thus affects the received signal producing its own image. For antisymmetric modes, on the other hand, the normal stress is zero at the interface, hence the scratch does not have any effect on the normal stress distribution of the plate. For 5.1 and 4.58 km/sec phase velocities, the shear stress at the interface plane is also small close to zero, thus the scratch does not have any effect on the shear stress distribution. Hence, one cannot see the image of the scratch for anti-symmetric modes for 17° and 19° incident angles. For 21° incidence or 4.16 km/sec phase velocity, the shear stress at the interface for the A_1 mode is larger than that for the A_2 mode (see Figs 9a and 9c). That is why the image of the scratch is clearer for the A_1 mode than the A_2 mode.

CONCLUDING REMARKS

In this paper the use of Lamb modes for interface characterization is investigated. It is found that modes which produce a large shear stress at the interface position are sensitive to the shear stiffness of the interface. Modes which produce large normal stresses but zero shear stress at the interface position are not at all sensitive to the shear stiffness of the interface. Interface defects, such as voids, which release the normal and shear stresses at the interface, can be detected by the modes which produce large normal or shear stresses

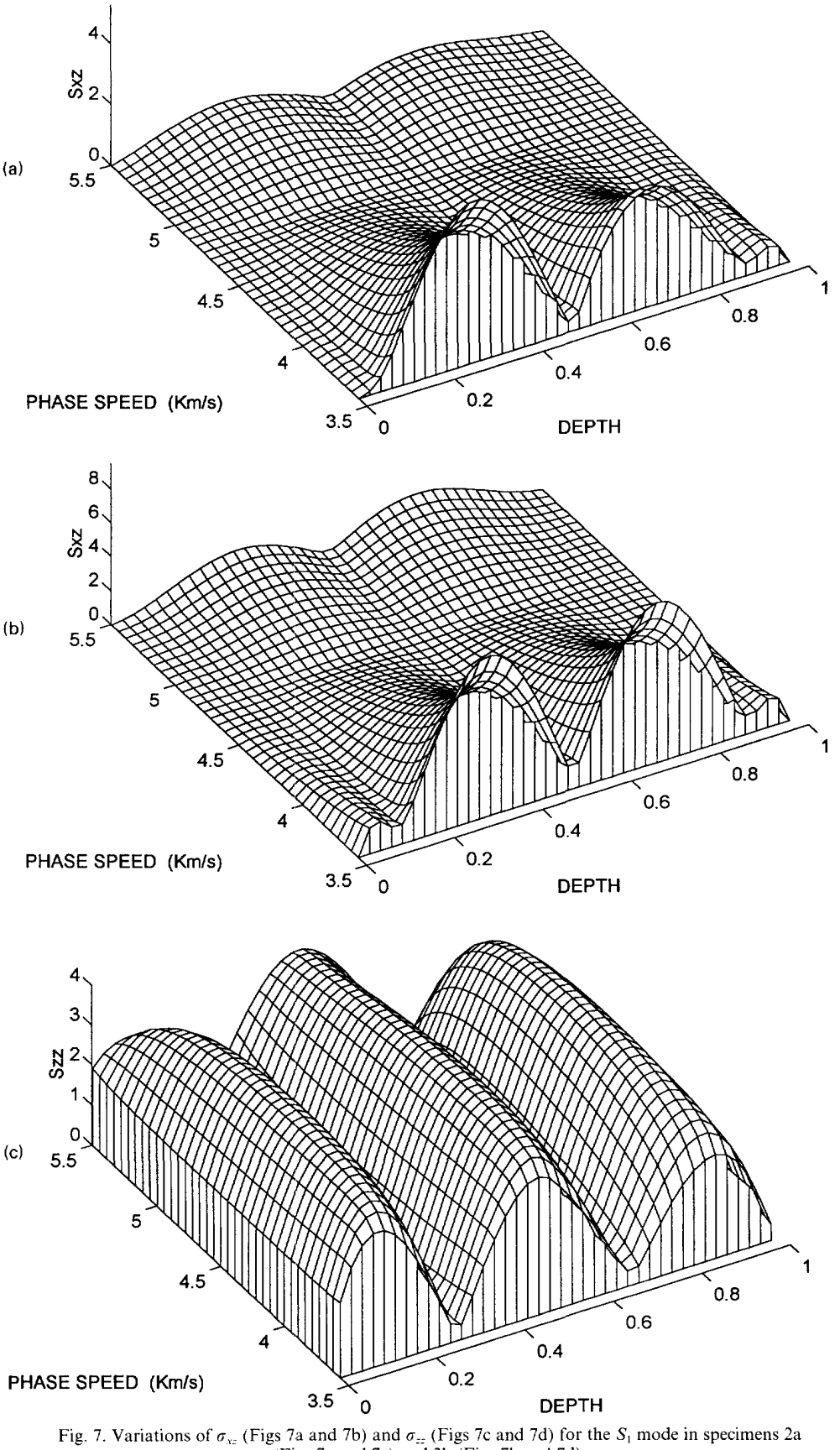

Fig. 7. Variations of σ_{xz} (Figs 7a and 7b) and σ_{zz} (Figs 7c and 7d) for the S_1 mode in specimens 2a (Figs 7a and 7c) and 2b (Figs 7b and 7d).

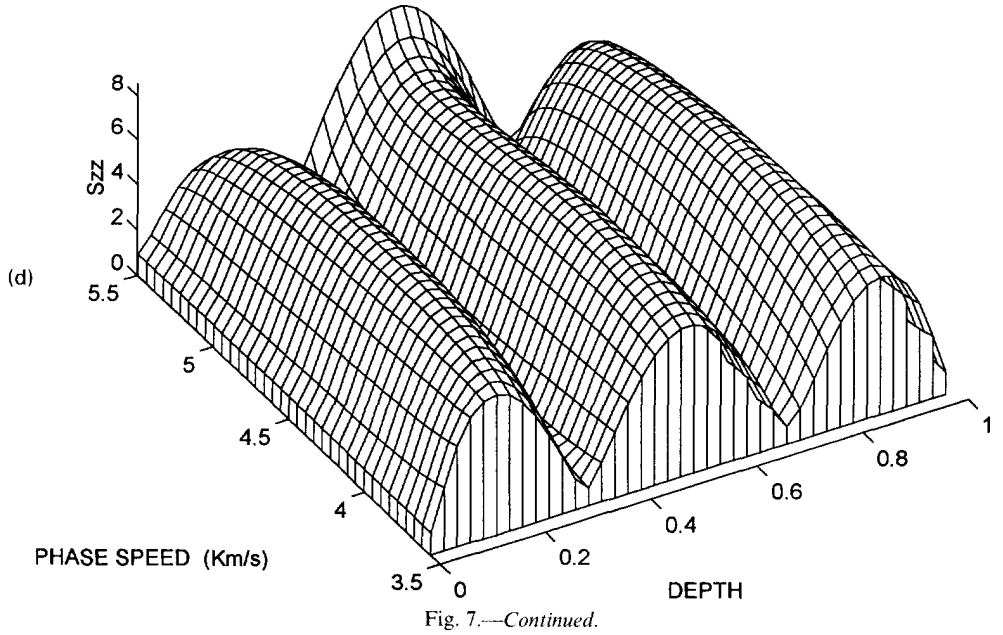

Fig. 7.—*Continued.*

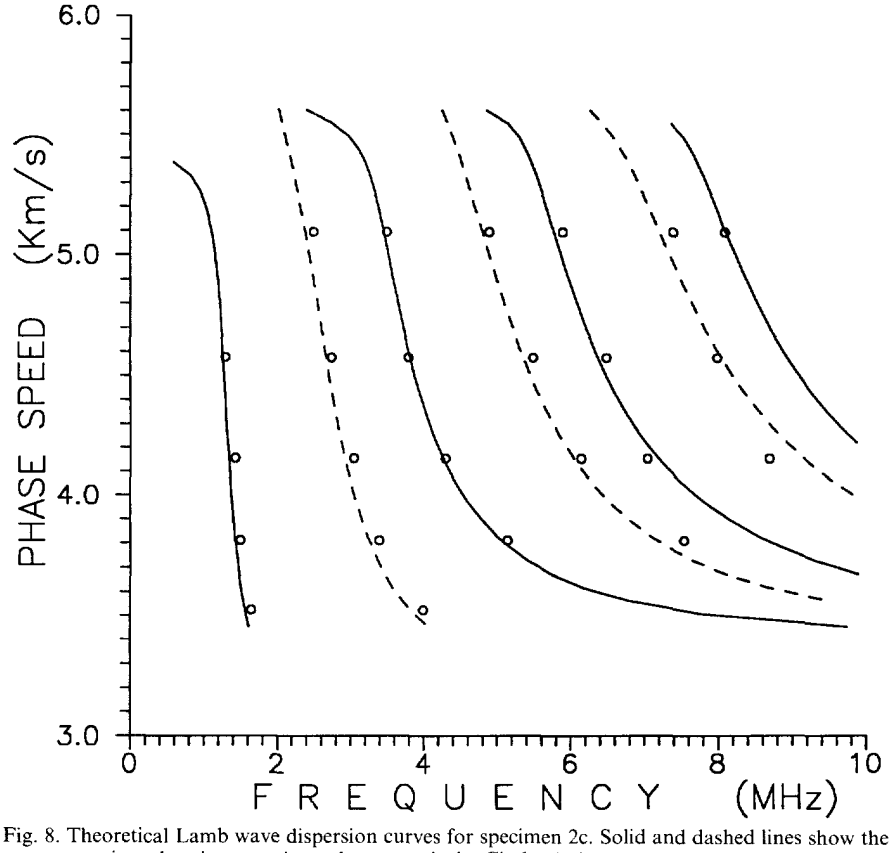

Fig. 8. Theoretical Lamb wave dispersion curves for specimen 2c. Solid and dashed lines show the symmetric and antisymmetric modes respectively. Circles (○) are experimental data points.

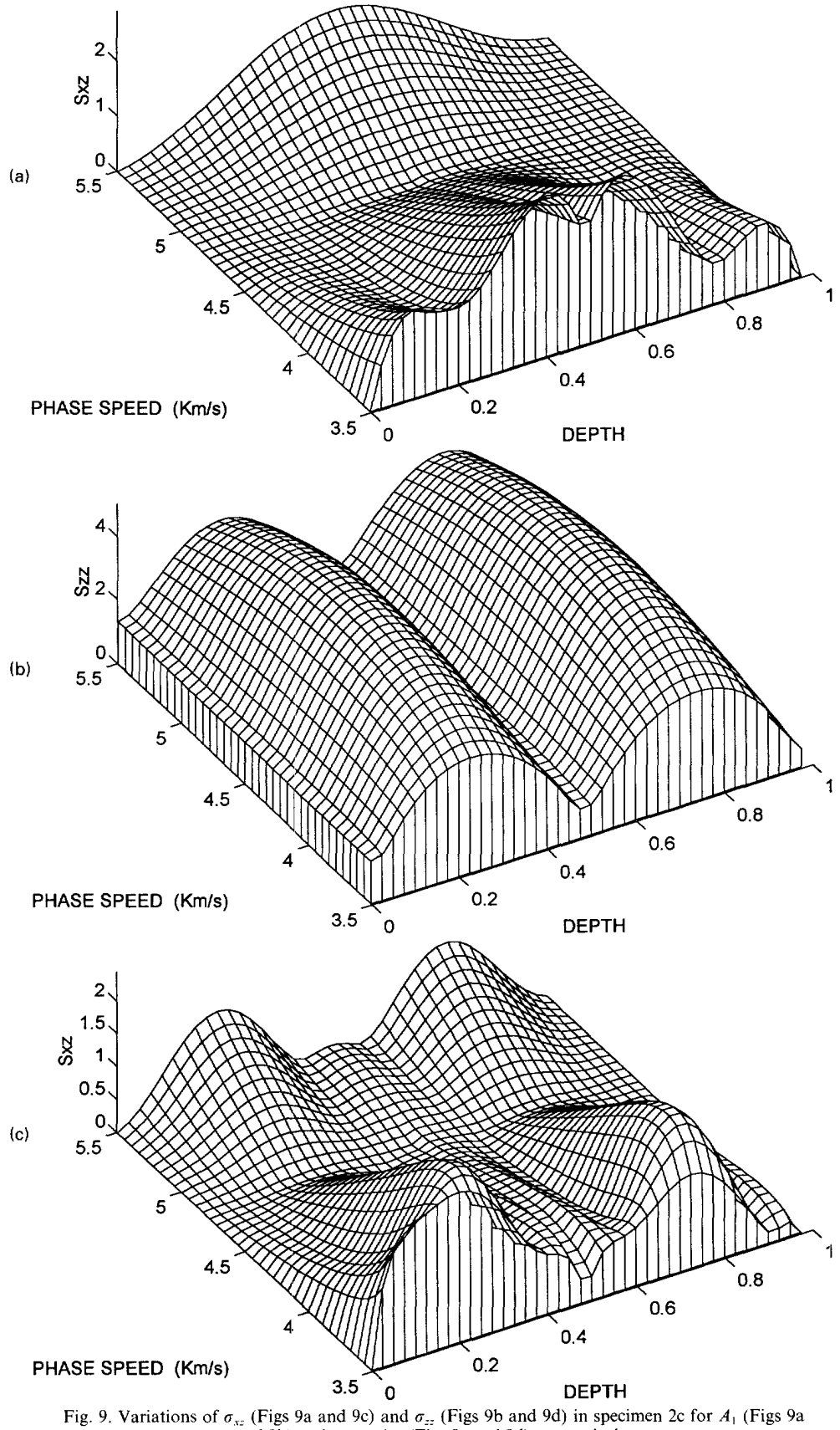

Fig. 9. Variations of σ_{xz} (Figs 9a and 9c) and σ_{zz} (Figs 9b and 9d) in specimen 2c for A_1 (Figs 9a and 9b) and A_2 modes (Figs 9c and 9d), respectively.

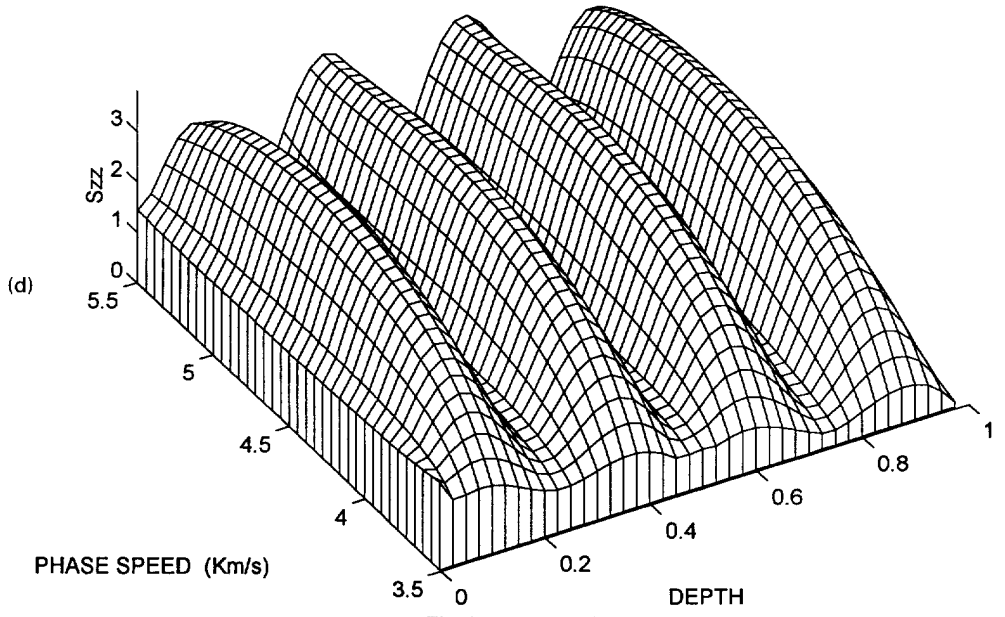

Fig. 9.—*Continued.*

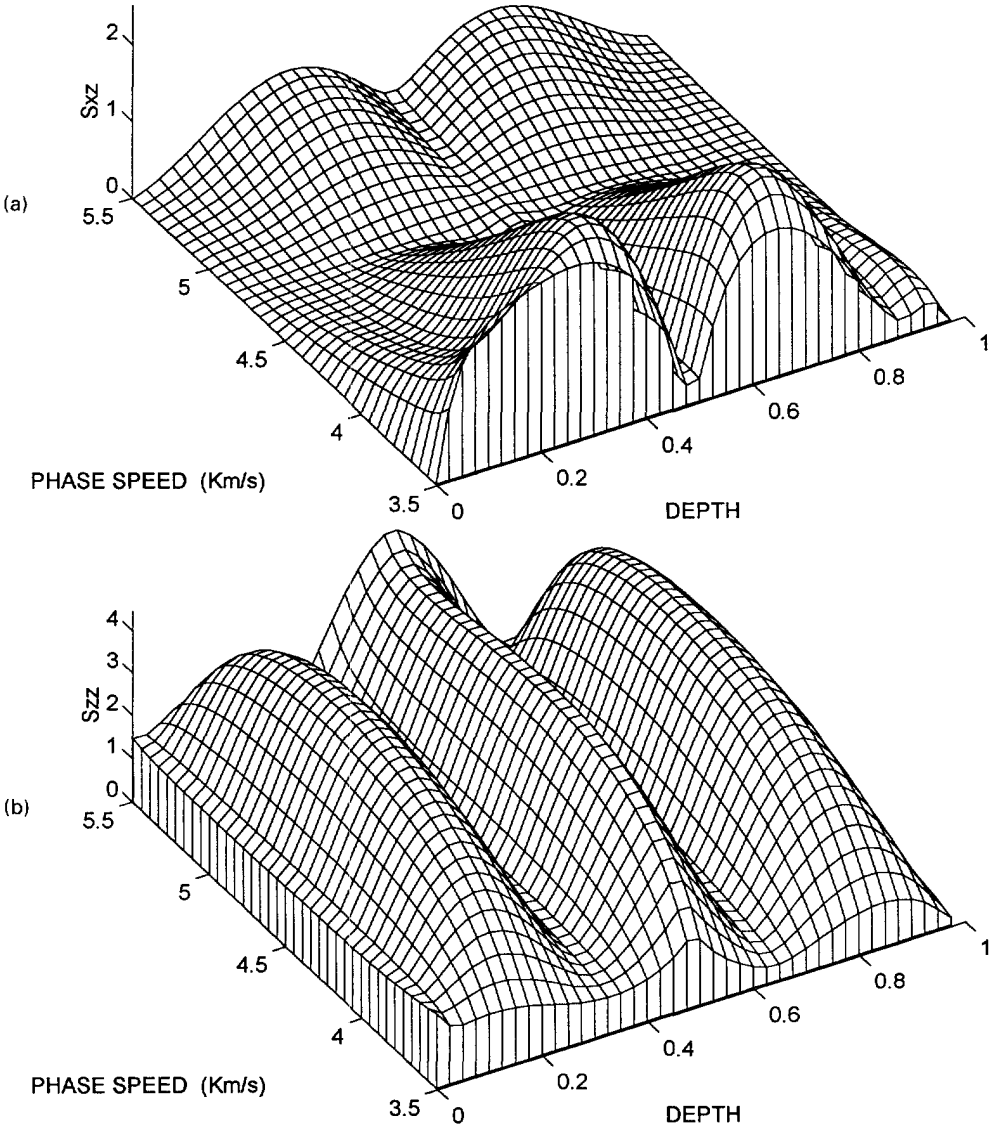

Fig. 10. Variations of σ_{xz} (Fig. 10a) and σ_{zz} (Fig. 10b) in specimen 2c for the S_1 mode of excitation.

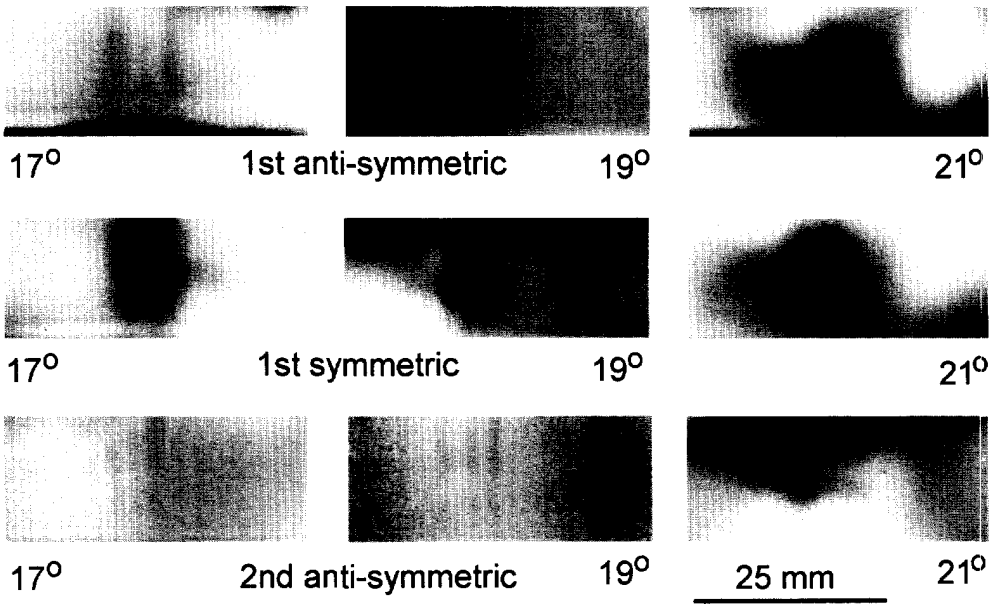

Fig. 11. Images of specimen 2c generated by different Lamb modes—A_1 (top row), S_1 (middle row), and A_2 (bottom row), for three different angles of incidence 17° (left column), 19° (middle column), and 21° (right column). Note that image of the scratch is clearly visible in the middle row.

at the interface. Normal and shear stress distribution for different Lamb modes show that the normal stress along the depth of the plate does not vary much when only the phase velocity is changed for the same mode. However, the shear stress variation along the depth of the plate is very sensitive to the phase velocity. In this case, one not only should specify which Lamb mode to use but also should mention the phase velocity (or frequency) that must be used for efficient scanning and characterization of the interface.

Acknowledgment—This research was supported by a grant from the National Science Foundation, CMS-9523349 and NATO Linkage grant, HTECH.LG931353.

REFERENCES

Brekhovskikh, L. M. and Gobin, O. A. (1990). *Acoustics of Layered media, Plane and Quasi-Plane Waves*, Springer-Verlag, Berlin, pp. 87–103.

Briggs, A. (1992). *Acoustic Microscopy*, Clarendon press, Oxford, U.K. pp. 102–103.

Chimenti, D. E. and Martin, R. W. (1991). Nondestructive evaluation of composite laminates by leaky Lamb waves. *Ultrasonics* **29,** 13–21.

Dunkin, J. W. (1965). Computation of modal solutions in layered elastic media at high frequencies. *Bull. Seismological Soc. Am.* **55,** 335–358.

Haskell, N. A. (1953). The dispersion of surface waves on multilayered media. *Bull. Seismological Soc. Am.* **43,** 17–34.

Jiao, D. and Rose, J. L. (1991). An ultrasonic interface layer model for bond evaluation. *J. Adhesion Sci. Tech.* **5,** 631–646.

Karpur, P., Benson, D. M., Matikas, T. E., Kundu, T. and Nicolaou, P. D. (1995). An approach to determine the experimental transmitter-receiver geometry for the reception of leaky Lamb waves. *Materials Evaluation* **53,** 1348–1352.

Kundu, T. (1992). A complete acoustic microscopical analysis of multilayered specimens. *ASME J. Appl. Mech.* **59,** 54–60.

Kundu, T. and Mal, A. K. (1985). Elastic waves in a multilayered solid due to a dislocation source. *Wave Motion* **7,** 459–471.

Kundu, T., Maslov, K., Karpur, P., Matikas, T. E. and Nicolaou, P. D. (1996). A Lamb wave scanning approach for mapping of defects in [0/90] titanium matrix composites. *Ultrasonics* **34,** 43–49.

Lévesque, D. and Piché, L. (1992). A robust transfer matrix formulation for the ultrasonic response of multilayered absorbing media. *J. Acoustical Soc. Am.* **92,** 452–467.

Mal, A. K. (1988). Wave propagation in layered composite laminates under periodic surface loading. *Wave Motion* **10,** 257–266.

Mal, A. K., Yin, C.-C. and Bar-Cohen, Y. (1991). Ultrasonic nondestructive evaluation of cracked composite laminates. *Composite Engng* **1,** 85–101.

Maslov, K. and Kundu, T. (1997). Selection of lamb modes for detecting internal defects in composite laminates. *Ultrasonics* (in press).

Matikas, T. E. and Karpur, P. (1993). Ultrasonic reflectivity technique for the characterization of fiber-matrix interface in metal matrix composites. *J. Appl. Physics* **74,** 228–236.

Schwab, F. and Knopoff, L. (1970). Surface wave dispersion computation. *Bull. Seismological Soc. Am.* **60,** 321–344.

Taylor, T. W. and Nayfeh, A. H. (1992). Dynamic internal response of fluid-loaded multilayered anisotropic media. *J. Acoustical Soc. Am.* **91,** 2519–2528.

Thomson, W. T. (1950). Transmission of elastic waves through a stratified solid medium. *J. Appl. Physics* **21,** 89–93.

Yang, W. and Kundu, T. (1997). Guided waves in multilayered anisotropic plates for internal defect detection. *ASCE J. Engng Mech.* (submitted).